Tellus (2000), 52B, 335–347
Printed in UK. All rights reserved

TELLUS
ISSN 0280–6509

Entrainment rates during ACE-2 Lagrangian experiments calculated from aircraft measurements

By MICHAEL J. SOLLAZZO[1], LYNN M. RUSSELL[1]*, DEREK PERCIVAL[2], SIMON OSBORNE[2], ROBERT WOOD[2] and DOUGLAS W. JOHNSON[2], [1]*Department of Chemical Engineering, Princeton University, Princeton, New Jersey;* [2]*Meteorological Research Flight, Farnborough, UK*

(Manuscript received 4 January 1999; in final form 13 September 1999)

ABSTRACT

Exchange rates of aerosol particles and vapor species between layers in the atmosphere allow us to estimate the lifetime of particles in the lower troposphere. This work analyzes data obtained during the ACE-2 campaign to calculate exchange using two independent methods, divergence and flux. The net entrainment rates obtained from the divergence method are based on spatially-integrated horizontal winds as well as on the average boundary layer height change. The flux method is based on an eddy correlation approach, but relies in this case on a point measurement of concentration change across an atmospheric interface. The thermodynamic structure in these three experiments included well-mixed layers in addition to overlying, more-stratified buffer layers, between which we have studied the net entrainment of air between adjacent layers. The range of entrainment rate magnitudes reported from both methods was from 0.000 m s^{-1} to 0.050 m s^{-1} (with the exception of a few outlying values). Since both methods have significant uncertainties, we believe the best estimates are the average net entrainment rates for both methods, which were 0.007, 0.007, and 0.006 m s^{-1} at the subsidence inversion, for Lagrangians 1, 2, and 3, respectively. The uncertainties were high for both methods, involving a factor of two uncertainty for entrainment rates below 0.020 m s^{-1}. This high uncertainty suggests that continued use of multiple independent methods for measuring entrainment, preferably with the aid of improved instrumentation for fast measurement of conserved tracers and well-designed sampling strategies, is essential for improving models of the sources and sinks for chemical evolution. In some cases, net entrainment rates calculated from the 2 methods were comparable, but in others the spatial inhomogeneity and sampling limitations led to significant discrepancies in the predicted rates.

1. Introduction

Determining the scattering of radiation in the atmosphere requires characterizing aerosol properties, especially in the troposphere. Both in-situ and satellite-sensed characteristics of aerosol properties have been shown to differ significantly around the Earth in recent field measurement campaigns (Durkee et al., 2000). Since the composition of aerosol particles varies with altitude and location in the atmosphere, their chemical properties are important for quantifying atmospheric cooling effects (Russell et al., 1994). In order to determine these properties, the rate of transfer between different layers in the atmosphere, in particular between the boundary layer and the free troposphere, must be known.

An important factor in determining the regional aerosol composition is the rate at which new particles are transferred into or removed from the boundary layer. Entrainment of particles into the boundary layer in typical North Atlantic

* Corresponding author: A317 Engineering Quadrangle, Princeton University, Princeton, NJ 08544, USA.
e-mail: lrussell@princeton.edu

conditions has been shown to dominate the evolution of anthropogenic aerosol particles by dilution (Van Dingenen et al., 1999, 2000). Van Dingenen et al. (1999, 2000) have shown that the entrainment mechanism can be more efficient than nucleation, condensation, cloud-processing, and coagulation processes in determining the shape of the typically observed bimodal marine particle size distribution. Previous work has also suggested that entrainment may provide a source of new particle production to the marine boundary layer by transport from nucleating regions in the free troposphere (Raes et al., 1993; Raes, 1995). In order to determine the quantitative role of entrainment in all of these aspects of aerosol evolution, we must calculate the rate of exchange of air into and out of the marine boundary layer.

Our approach and accuracy in measuring entrainment rates varies both with the regional meteorology and with the instrumentation and sampling approach employed. In regions where slowly varying, horizontally homogeneous boundary layers persist, three aircraft-based methods — divergence, flux, and budget approaches — have been employed by Lenschow et al. (1999) and Russell et al. (1998). Both works considered entrainment rates measured in remote regions of the Southern Ocean in November and December of 1995 during ACE-1 (Bates et al., 1998). Lenschow et al. (1999) show that the flux method approach of quantifying the covariance of a conserved tracer with vertical wind is likely to be the most accurate when the jump across the boundary layer interface is measurably large and is sampled sufficiently to characterize its variability. Russell et al. (1998) illustrate that in the absence of sufficient sampling, the divergence method or the budget method is likely to produce more consistent results in regions that are not disturbed by frontal events.

For the Second Aerosol Characterization Experiment (ACE-2), the region studied was the eastern North Atlantic, bounded by Portugal, northwest Africa, the Canary Islands, and the Azores (Raes et al., 2000; Verver et al., 2000). The meteorology of this area has been characterized by several previous aircraft studies (Nicholls, 1984; Albrecht et al., 1985; Martin et al., 1994; Bretherton et al., 1995), with observations of extensive stratocumulus coverage during the summer months including intermittent cumulus formation.

This complex structure and the associated clouds limit the accuracy of all of those approaches to quantifying entrainment between the free troposphere and lower layers. The flux method should be employed with a tracer that is conserved in cloud over a horizontally homogeneous region with multiple penetrations of the boundary layer top. The divergence method requires flying around a large region (at least 29 km radius) during a time with minimal changes in structure (Lenschow et al., 1999). The budget method requires one or more vertically-characterized tracers with quantified sources and sinks (Russell et al., 1998). In this paper, we compare the results obtained by the flux and divergence methods and investigate the impact of the North Atlantic region's meteorological inhomogeneity on the predicted results.

During ACE-2 in June and July of 1997, 3 sets of Lagrangian flights were performed by the Meteorological Research Flight (MRF) C-130 aircraft based in Tenerife (Raes et al., 2000; Johnson et al., 2000a). During these Lagrangian experiments, the aircraft drifted with the wind while flying in a square pattern, thereby moving with a particular air parcel that is tracked by a constant-altitude balloon launched into the air mass. The flight numbers and start times for all three Lagrangians are given by Johnson et al. (2000a). Each flight was 8 to 10 h long and included from three to nine closed-box patterns. These boxes were divided into one or two stacks at varying altitudes, consisting of squares flown at a typical speed of 100 m s^{-1} with 270° standard-rate turns for the corners at each altitude. In addition to these square patterns, profiles were flown from approximately 7000 m to 30 m above sea level. The data collected during the square patterns and the profiles were used to calculate entrainment rates. The two methods employed are described in Section 2.

2. Entrainment calculations

In a Lagrangian framework, the change in concentration for a scalar quantity $\mathscr{S} = S + s$, where S is the mean concentration and s is the

fluctuation from the mean, can be given by:

$$\frac{\partial S}{\partial t} + \frac{\partial \overline{ws}}{\partial z} + W\frac{\partial S}{\partial z} = Q_s, \quad (1)$$

where $\overline{ws}$ (the vertical eddy flux of $\mathscr{S}$) is the average of the product ws over the sampling time, Q_s is the internal (chemical) source or sink of $\mathscr{S}$, and W_z is the mean vertical velocity at some level z. We assume that the Lagrangian experiments during ACE-2 each tracked a unique and homogeneous air mass for the 36-h period during which the balloons were followed. In considering rates of exchange among layers in this moving column of air, different velocities in each layer result in ambiguity as the balloon tracks accurately only the layer in which it resides. Significant differential advection cannot be taken into account by this approach, although small variations in layer velocities are negligible if layers are sufficiently homogeneous.

Here, we will study a net entrainment velocity, namely the net rate at which fluid passes from one layer to another across an interface A at height h_A where this velocity is given by

$$w_e^A = \frac{\partial h_A}{\partial t} - W_{h_A}. \quad (2)$$

In cases in which exchange occurs in both upward and downward directions, the net entrainment defined here is the difference between the 2 velocities with the positive direction defined to be downward. For an interfacial layer of infinitesimal thickness, described by the altitude difference $h_{A+} - h_{A-}$, eq. (1) can be integrated to give

$$\delta\overline{ws}_A = \left(\frac{\partial h_A}{\partial t} - W_{h_A}\right)\delta S_A = w_e^A \delta S_A, \quad (3)$$

where δS_A is the difference in concentration across interface A and

$$\delta\overline{ws}_A = (\overline{ws})_{h_{A+}} - (\overline{ws})_{h_{A-}}, \quad (4)$$

as derived by Russell et al. (1998). Thus, the net entrainment velocity across layer A by the flux method is given by

$$w_e^A = \frac{(\overline{ws})_{h_{A+}}}{\delta S_A} - \frac{(\overline{ws})_{h_{A-}}}{\delta S_A}. \quad (5)$$

This relationship forms the basis of the flux method calculation.

The approach to calculating the net entrainment rate by the divergence method requires measurements of the mean vertical motion at the height of the interface, W_{h_A}, as well as the time rate of change of the layer interface, $\partial h_A/\partial t$ as described in eq. (2). The mean horizontal divergence at several levels below the interface at h_A can be integrated to the level of the boundary layer interface to obtain W_{h_A} as described by

$$W_{h_A} = \int_0^{h_A} \frac{\partial \tilde{w}}{\partial z}\,dz = -\int_0^{h_A}\left(\frac{1}{\mathscr{A}}\oint v_n\,dl\right)dz \quad (6)$$

where $\mathscr{A}$ is the area enclosed by the integration path over the differential path segment dl, $\tilde{w}$ is the average vertical velocity within the integration path, and v_n is the horizontal velocity component normal to the path of integration, and we have used zero mean vertical velocity at the surface (Lenschow, 1996; Russell et al., 1998).

2.1. *Divergence method*

To evaluate the above relationships for entrainment, we measured the rate at which the height of a layer interface changes with time and the rate of subsidence at this interface (Lenschow, 1996; Russell et al., 1998; Lenschow et al., 1999). The change in height with time was obtained from curve fits of individual measurements of boundary layer height during vertical profiles through the lower troposphere.

For subsidence, we first calculated divergence by integrating the component of the wind normal to the flight path around a closed loop. Corners and any extra points at the beginning or end of the flight were removed from the data before calculating divergence. Using the resulting approximately-closed loop, the perimeter was used to infer the area of the enclosed quadrangle. Then, the component of wind speed normal to the flight path was integrated around the box and divided by the area to give the divergence as given in eq. (6). In order to define downward vertical velocity as positive consistently in the divergence calculation, we have used the convention that clockwise motion and outward lateral wind components are positive. For each box, we obtained a value for the divergence at the sampled altitude. Linear fits of divergence rates with altitude were calculated by least squares using three to five boxes for each stack.

In order to correct for the instrument bias in the direction of flight in the differential pressure measurements, average clockwise and counter-

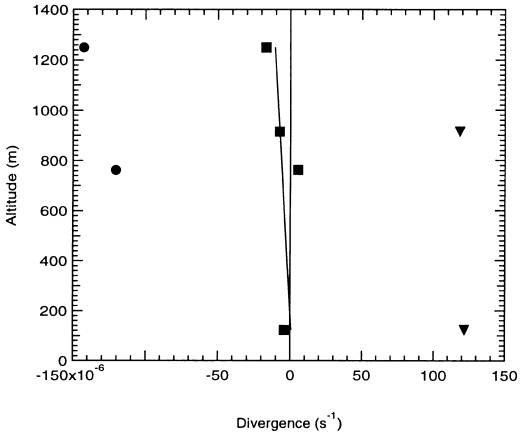

Fig. 1. Raw and corrected divergences from stack 2 of flight A568 during Lagrangian 3. Circles indicate uncorrected counterclockwise measurements, triangles indicate uncorrected clockwise measurements, and the squares represent the divergence values after correction by removing the average directional bias. The solid line represents the curve fit of the corrected divergence measurements used to evaluate the divergence at the layer interfaces.

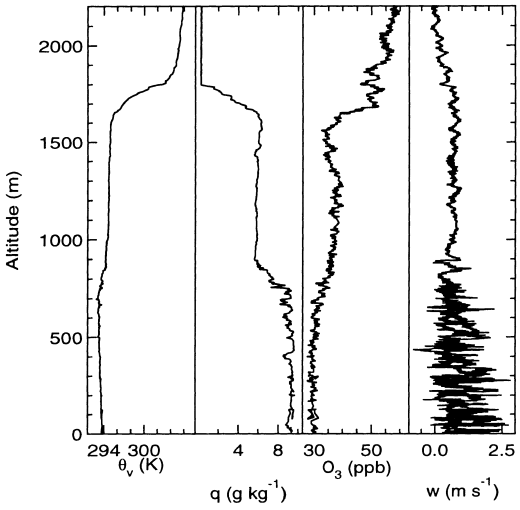

Fig. 2. An example of the measured values of virtual potential temperature θ_v, water mixing ratio q, ozone O_3, and vertical wind component w for a profile flown for Lagrangian 1 at JDT 185.50 (1153 July 4).

clockwise differences were determined for each flight, and this correction was subtracted from all values (Lenschow, 1996). The corrected divergence values were plotted against altitude in order to integrate from the surface to the boundary layer height, an example of which is shown in Fig. 1 for flight A568, stack 2. The large directional instrument bias (which is seen in Fig. 1 to be on the order of the values reported) for the boxes sampled here contributes to the uncertainty of this approach since the resulting differences are small relative to the correction applied. By interpolating between the measured box altitudes and integrating from the surface to the boundary layer top we have obtained subsidence using eq. (6) and entrainment from eq. (2).

2.2. *Flux method*

Entrainment rates can also be calculated using the covariance of a tracer with vertical wind fluctuations at the interface with the jump in tracer concentration across the boundary layer (Lilly, 1968; Kawa and Pearson, 1989; Lenschow, 1996; Russell et al., 1998; Wang et al., 1999). For the flux method, the tracer measured by the MRF C130 at high sampling frequency (32 Hz) that is conserved in most of the conditions studied in the cloudy but primarily non-precipitating (with the exception of part of Lagrangian 2) conditions encountered during ACE-2 is water mixing ratio.

For water mixing ratio, the jump in concentration across the interface at the top of the boundary layer was determined by identifying the boundary layer height and calculating the difference in the average tracer concentration above and below the interface. The profiles of water vapor mixing ratio, virtual potential temperature, ozone concentration, and vertical wind are shown in Figs. 2, 6, and 10. Mixing ratio (q) was determined from total water dew point temperatures. Virtual potential temperature (θ_v) and ozone (O_3) concentration were used to identify the layer boundaries. In the predominantly and persistently cloudy conditions encountered during all three Lagrangian experiments (Johnson et al., 2000b; Osborne et al., 2000; Wood et al., 2000), virtual potential temperature is not conserved because of condensation of water and radiational divergence and consequently was not useful as a tracer. The top of the boundary layer was identified where the fluctuations in the vertical wind indicated a decrease in turbulent mixing and the tracer concentrations showed discontinuous jumps. The jump in water mixing ratio across the boundary layer top (δS_A) was quantified

by taking an average of points in a 50 m range above and below the boundary.

The covariance of water vapor mixing ratio with vertical wind was calculated by summing the cospectra, namely the real part of the Fourier transform of the detrended tracer multiplied with the conjugate of the Fourier transform of the vertical wind. Contributions to the covariance from scales too small and too large to be sampled sufficiently were removed by limiting the frequency range considered to the range from 0.01 to 16 Hz.

The covariance values were plotted with altitude for each stack in order to interpolate to the values above and below the interface. In many cases, the intermediate and top layers had only one value measured in the layer in which case the slope was taken to be identical to a contemporary measurement in another layer which did include multiple values; the resulting error in the slope estimates account for the large uncertainties reported in Table 2 (Russell et al., 1998). At each interface, the upward and downward entrainment rates are given by eq. (5).

3. Lagrangian 1

During Lagrangian 1, a relatively deep boundary layer capped by a subsidence inversion was observed which was made up of two layers, a buffer layer below interface *B* with scattered cumulus clouds and broken stratocumulus which was decoupled from the surface by a well-mixed surface-based layer below interface *A*. The transition region at interface *A* was up to 100 m deep. The cloud layer showed a decrease in height with time while the surface-based mixed layer experienced a gradual increase as described in Johnson et al. (2000b). A typical profile for this set of Lagrangian flights is shown in Fig. 2. The heights of the layers were obtained by fitting polynomial functions to time series of temperature inversion altitudes and mixing heights as described in Johnson et al. (2000b). The curve fits used to illustrate the evolution of the boundary layer during these flights are shown in Fig. 3 and are given by eqs. (7) and (8):

$$h_A(t) = -1.50088193 \times 10^7 + 1.61279993 \times 10^5 t - 4.33239981 \times 10^2 t^2 \quad (7)$$

$$h_B(t) = -1.38892194 \times 10^7 + 1.50309993 \times 10^5 t - 4.06629982 \times 10^2 t^2 \quad (8)$$

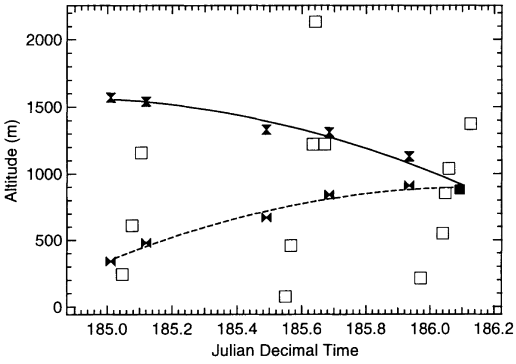

Fig. 3. Heights of layer interfaces for Lagrangian 1. Squares indicate the times and positions of box patterns flown by the C130 aircraft during the experiment. Measured values of the layer boundaries from aircraft profiles are indicated by symbols (bowties for interface *A*, hourglasses for interface *B*). The curve fits applied for their change with time are shown by lines (dashed line for interface *A*, solid line for interface *B*).

where t is given in Julian Decimal Time and h is in m. The decrease in height of approximately 600 m in 24 h of interface *B* indicates a quite rapid change in the layer structure.

For the surface-based mixed layer (below interface *A*), the results of the two methods showed some agreement for flight A551, but predicted opposite trends during flight A553 as shown in Fig. 4. The divergence method is estimated to have a higher error in all three flights, but for flight A553 the covariance-based entrainment also has significant errors due to the small jump of $-1.16\ \mathrm{g\,kg^{-1}}$ in mixing ratio at interface *A*. For the buffer layer under the subsidence inversion (interface *B*), Fig. 5 shows a peak value of $0.023\ \mathrm{m\,s^{-1}}$ at JDT 185.5 (1200, 4 July). The mixing ratio flux method predicted $-0.024\ \mathrm{m\,s^{-1}}$ for JDT 185.9 (2130, 4 July), providing a contradiction in the predicted direction of entrainment. The latter estimate of net upward entrainment is more likely since the rapid decrease in height of interface *B* would require an uncommonly high subsidence rate to account for the net downward entrainment predicted by the divergence method.

For divergence-based estimates, initial entrain-

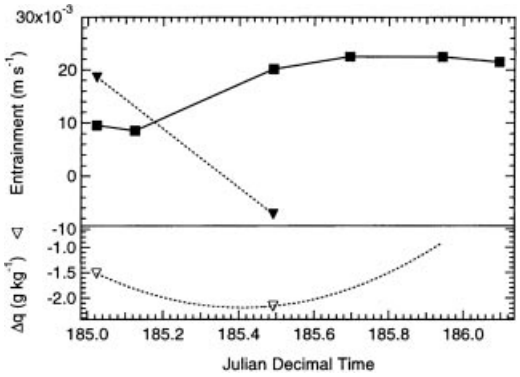

Fig. 4. Calculated entraiment rates and concentration differences at interface *A* for Lagrangian 1. Squares indicate values calculated by the divergence method, and triangles indicate values calculated by the flux method. In this graph, the final entrainment rate calculated with the flux method of -3.3×10^{-1} m s^{-1} at JDT 185.94 does not appear as it is out of the displayed range of entrainment rates.

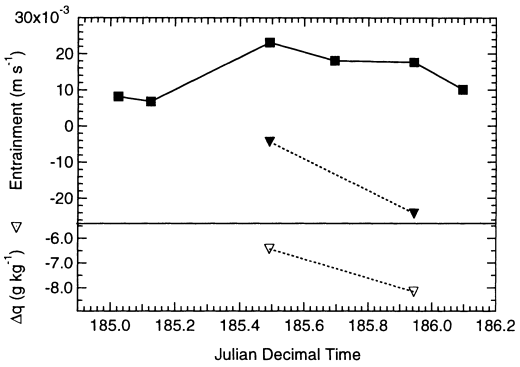

Fig. 5. Same as in Fig. 4 at interface *B* for Lagrangian 1.

ment rates at interface *A* of approximately 0.01 m s^{-1} were obtained across both interfaces, and the entrainment rates were predicted to increase during the Lagrangian to over 0.02 m s^{-1}. As the subsidence inversion decreased in height from 1500 to 900 m in altitude, air was entrained at a continuously increasing rate from the free troposphere into the boundary layer during the 36-h study period.

4. Lagrangian 2

The boundary layer heights for Lagrangian 2 are shown in Fig. 7, and a typical profile is shown in Fig. 6, revealing a relatively large increase in the height of the boundary layer between flights A558 and A559 (Osborne et al., 2000). For the main subsidence inversion (interface *B*), an increase in height is observed as illustrated in Fig. 7. We have fit the change in height of the boundary layer determined from temperature inversions and mixing heights as described by Osborne et al. (2000) with a polynomial to give eq. (9) for interface *A*:

$$h_A(t) = -1.19612956 \times 10^7 + 1.20489963 \times 10^5 t - 3.03424922 \times 10^2 t^2. \quad (9)$$

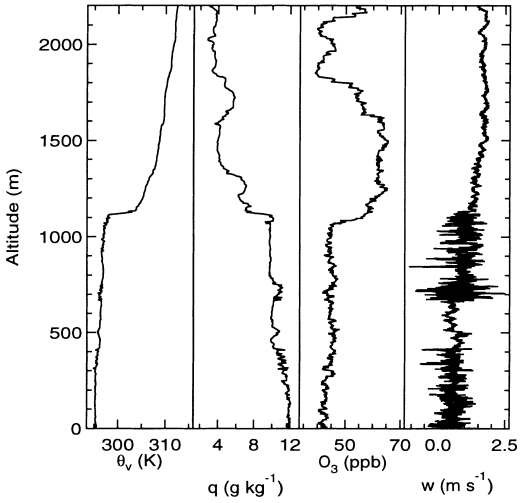

Fig. 6. Same as in Fig. 2 for Lagrangian 2 at JDT 198.95 (2248 July 17).

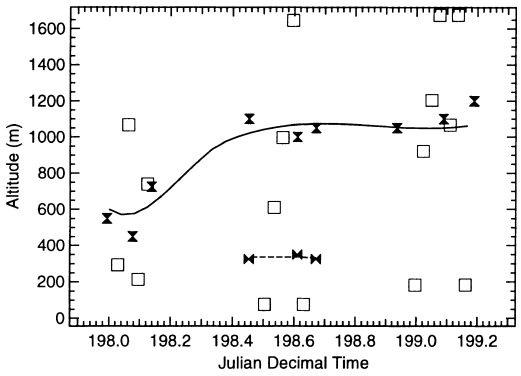

Fig. 7. Same as in Fig. 3 for Lagrangian 2.

Layer B was fit with eq. (10) for $198.0 < t < 198.3$:

$$\begin{aligned} h_B(t) = & -2.16231070 \times 10^{10} \\ & -1.09241597 \times 10^{8} t \\ & -5.49399222 \times 10^{5} t^2 \\ & +6.28014155 \times 10^{0} t^3 \\ & +1.39908152 \times 10^{1} t^4 \\ & +7.03629719 \times 10^{-2} t^5 \\ & -3.55478181 \times 10^{-4} t^6 \end{aligned} \quad (10)$$

and with eq. (11) for $t > 198.3$:

$$\begin{aligned} h_B(t) = & -9.60291551 \times 10^{9} \\ & +1.44866991 \times 10^{8} t \\ & -7.28474143 \times 10^{5} t^2 \\ & +1.22106073 \times 10^{3} t^3. \end{aligned} \quad (11)$$

Figs. 8 and 9 show the entrainment rates predicted by the divergence and flux methods for the layers below interfaces A and B, respectively. The height–time series with the graph of entrainment rates for the layer below interface B shows that the greatest entrainment of 0.023 m s^{-1} occurs where the boundary layer height is increasing fastest at JDT 198.15 (0330, 17 July). Values for entrainment approach zero as the layer stops increasing in height.

This large entrainment is consistent with a rapid addition of air to the boundary layer. Since mixing ratio is not conserved in drizzling cloud, we expect the flux method to be less reliable in this case.

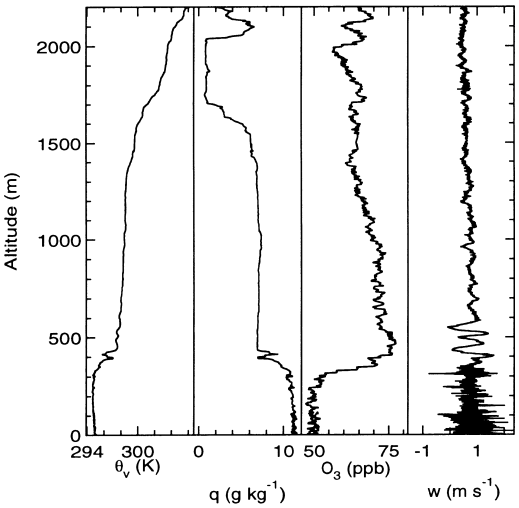

Fig. 10. Same as in Fig. 2 for Lagrangian 3 at JDT 204.94 (2234 July 24).

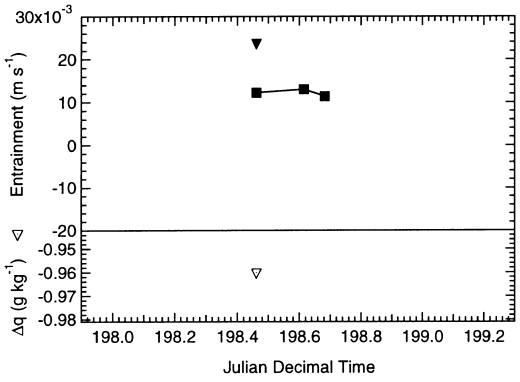

Fig. 8. Same as in Fig. 4 at interface A for Lagrangian 2.

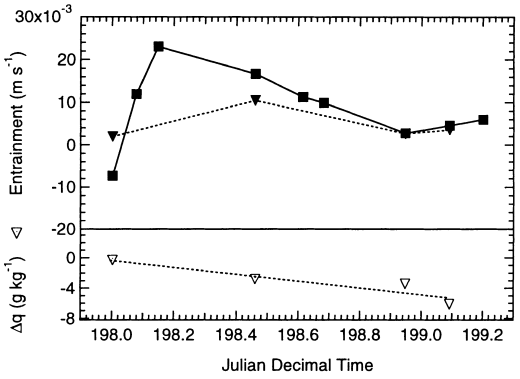

Fig. 9. Same as in Fig. 4 at interface B for Lagrangian 2.

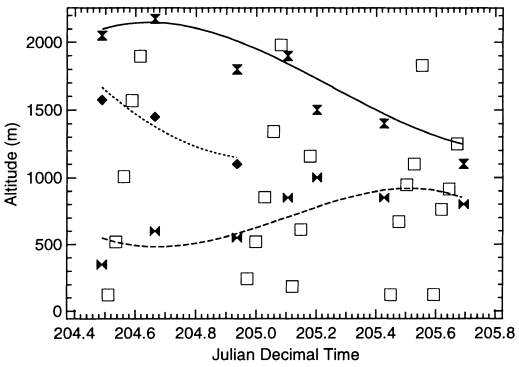

Fig. 11. Heights of layer interfaces for Lagrangian 3. Squares indicate the times and positions of box patterns flown by the C130 aircraft during the experiment. Measured values of the layer boundaries from aircraft profiles are indicated by symbols (bowties for interface A, diamonds for interface B, hourglasses for interface C). The curve fits applied for their change with time are shown by lines (dashed line for interface A, solid line for interface B, dotted line for interface C).

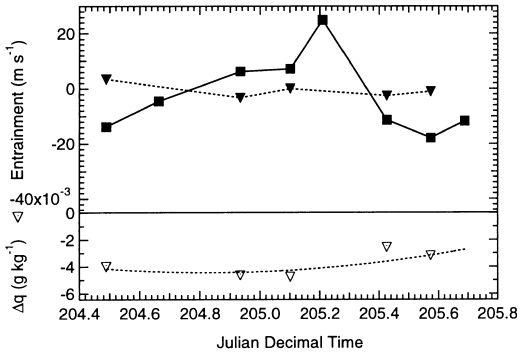

Fig. 12. Same as in Fig. 4 at interface *A* for Lagrangian 3.

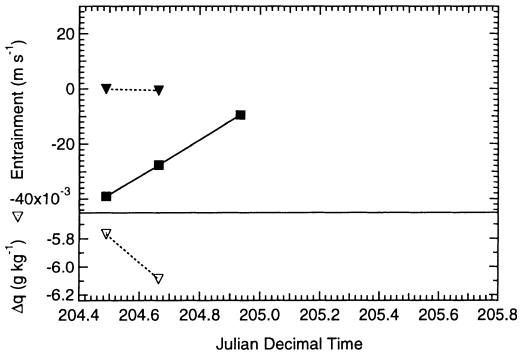

Fig. 13. Same as in Fig. 4 at interface *B* for Lagrangian 3.

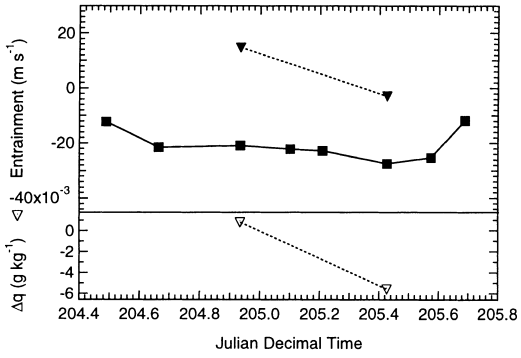

Fig. 14. Same as in Fig. 4 at interface *C* for Lagrangian 3.

Nevertheless, the mixing ratio-based flux method estimate of entrainment rate agrees well with the divergence method in both shape and magnitude. This agreement is consistent with the estimate of Osborne et al. (2000) that only 12% of a 0.00027 m d^{-1} precipitation rate was removed to the surface, minimizing the loss of the water tracer in this case.

In addition to the subsidence inversion, a decoupling creating a new layer below interface *A* was observed and may have persisted for more than 8 h (Osborne et al., 2000). Both methods predicted positive values of 0.011 to 0.024 m s^{-1} for entrainment at interface *A* as shown in Fig. 8. For this layer, only limited data were available for the covariance method, so no trend is available for this data set.

5. Lagrangian 3

For the last Lagrangian experiment, a two-layered system was observed initially but later a third layer formed between the original two that contained high concentrations of several anthropogenically-emitted species (Wood et al., 1999). An example of the temperature, tracer, and vertical wind measurements is shown in the profile in Fig. 10. Beginning with the internal boundary layer (below interface *A*), Fig. 11 shows a relatively constant height before a rapid increase from JDT 204.9 (2130, 23 July) to 205.2 (0450, 24 July). Changes in height of interfaces *A*, *B*, and *C* are based on temperature inversion and mixing heights determined by Wood et al. (2000), and here the hyperbolic and polynomial fits for the heights of the interfaces are given by eqs. (12), (13), and (14), respectively, where we have translated the time t to JDT to be consistent with the previous equation format.

$$h_A(t) = 712.5 + 237.5 \tanh[12t - 2461], \quad (12)$$

$$h_B(t) = +7.60715377 \times 10^7 - 7.42030611 \times 10^5 t + 1.80953889 \times 10^3 t^2, \quad (13)$$

$$h_C(t) = -1.076860196 \times 10^{10} + 1.57404511 \times 10^8 t - 7.66920269 \times 10^5 t^2 + 1.24554240 \times 10^3 t^3. \quad (14)$$

For interface *A*, a hyperbolic function has been used by Wood et al. (2000) instead of a polynomial in order to more accurately represent the change in height with time for this case.

Fig. 12 shows the entrainment rates calculated for Lagrangian 3. There is a large increase in the divergence-based entrainment rate calculated for the rapid rise in the internal boundary layer with these values increasing from 0.002 to 0.029 m s^{-1}.

Table 1. *Entrainment rates and associated error estimates during the ACE-2 Lagrangian experiments calculated by the divergence method*

Flight: stack, profile	JDT	Boxes per stack	Interface height, z_A (m)	Entrainment rate, w_e^A (m s^{-1})	Interface height, z_B (m)	Entrainment rate, w_e^B (m s^{-1})	Interface height, z_C (m)	Entrainment rate, w_e^C (m s^{-1})
Lagrangian 1								
A551: 1, 2	185.02	3	364	$9.5 \times 10^{-03} \pm 2.6 \times 10^{-02}$	1557	$8.1 \times 10^{-03} \pm 5.3 \times 10^{-02}$		
A551: 1, 4	185.13	3	457	$8.5 \times 10^{-03} \pm 2.9 \times 10^{-02}$	1537	$6.8 \times 10^{-03} \pm 5.3 \times 10^{-02}$		
A552: 1, 2	185.49	5	719	$2.0 \times 10^{-02} \pm 2.8 \times 10^{-02}$	1394	$2.3 \times 10^{-02} \pm 3.9 \times 10^{-02}$		
A552: 1, 4	185.69	5	814	$2.3 \times 10^{-02} \pm 3.0 \times 10^{-02}$	1268	$1.8 \times 10^{-02} \pm 3.7 \times 10^{-02}$		
A553: 1, 2	185.94	5	881	$2.3 \times 10^{-02} \pm 3.1 \times 10^{-02}$	1068	$1.8 \times 10^{-02} \pm 3.4 \times 10^{-02}$		
A553: 1, 3	186.10	5	896	$2.2 \times 10^{-02} \pm 3.1 \times 10^{-02}$	919	$1.0 \times 10^{-02} \pm 3.2 \times 10^{-02}$		
Lagrangian 2								
A558: 1, 2	198.00	4			595	$-7.3 \times 10^{-03} \pm 2.9 \times 10^{-02}$		
A558: 1, 3	198.08	4			575	$1.2 \times 10^{-02} \pm 2.8 \times 10^{-02}$		
A558: 1, 4	198.15	4			643	$2.3 \times 10^{-02} \pm 3.0 \times 10^{-02}$		
A559: 1, 2	198.46	5	336	$1.2 \times 10^{-02} \pm 1.9 \times 10^{-02}$	1026	$1.7 \times 10^{-02} \pm 3.4 \times 10^{-02}$		
A559: 1, 3	198.61	5	337	$1.3 \times 10^{-02} \pm 1.9 \times 10^{-02}$	1069	$1.1 \times 10^{-02} \pm 3.4 \times 10^{-02}$		
A559: 1, 4	198.68	5	333	$1.1 \times 10^{-02} \pm 1.9 \times 10^{-02}$	1073	$9.9 \times 10^{-02} \pm 3.4 \times 10^{-02}$		
A560: 1, 1	198.95	4			1053	$2.8 \times 10^{-03} \pm 3.8 \times 10^{-02}$		
A560: 1, 2	199.09	4			1051	$4.6 \times 10^{-03} \pm 3.8 \times 10^{-02}$		
A560: 2, 5	199.20	3			1070	$6.0 \times 10^{-03} \pm 4.4 \times 10^{-02}$		
Lagrangian 3								
A566: 1, 2	204.49	5	475	$-4.1 \times 10^{-03} \pm 2.3 \times 10^{-02}$	1667	$-3.9 \times 10^{-02} \pm 4.3 \times 10^{-02}$	2087	$-9.9 \times 10^{-03} \pm 4.8 \times 10^{-02}$
A566: 1, 3	204.66	5	475	$-4.1 \times 10^{-03} \pm 2.3 \times 10^{-02}$	1379	$-2.8 \times 10^{-02} \pm 3.9 \times 10^{-02}$	2158	$-2.1 \times 10^{-02} \pm 4.9 \times 10^{-02}$
A567: 1, 2	204.93	5	488	$2.4 \times 10^{-03} \pm 2.3 \times 10^{-02}$	1150	$-9.5 \times 10^{-03} \pm 3.6 \times 10^{-02}$	2023	$-2.2 \times 10^{-02} \pm 4.7 \times 10^{-02}$
A567: 1, 3	205.10	5	762	$2.9 \times 10^{-02} \pm 2.9 \times 10^{-02}$			1846	$-2.3 \times 10^{-02} \pm 4.5 \times 10^{-02}$
A567: 2, 4	205.21	3	928	$2.2 \times 10^{-02} \pm 4.1 \times 10^{-02}$			1713	$-2.3 \times 10^{-02} \pm 5.6 \times 10^{-02}$
A568: 1, 1	205.43	5	950	$-1.5 \times 10^{-02} \pm 3.2 \times 10^{-02}$			1446	$-2.8 \times 10^{-02} \pm 4.0 \times 10^{-02}$
A568: 1, 3	205.57	5	950	$-1.5 \times 10^{-02} \pm 3.2 \times 10^{-02}$			1297	$-2.6 \times 10^{-02} \pm 3.8 \times 10^{-02}$
A568: 2, 4	205.69	4	950	$-2.7 \times 10^{-03} \pm 3.2 \times 10^{-02}$			1217	$-1.1 \times 10^{-02} \pm 4.1 \times 10^{-02}$

The curve based on mixing ratio flux shows little correlation, with all values under 0.004 m s^{-1}.

For this layer, we have sufficient time histories of ozone and carbon monoxide (CO) to compare the entrainment rates derived from the budgets of these species to the flux-based entrainment rate for $w_e^{2\to1}$, namely the downward entrainment of air through interface *A* (Kawa and Pearson, 1989; Russell et al., 1998). Here, the flux method predictions initially decrease during the first flight from 0.004 to 0.001 m s^{-1}, before increasing slightly to 0.002 m s^{-1} at JDT 205.10 and then decreasing to below 0.001 m s^{-1}. Both O_3 and CO budgets initially predict higher entrainment rates at JDT 204.83 of 0.005 and 0.002 m s^{-1}, respectively, but also show increasing trends at JDT 205.10, predicting values up to 0.011 and 0.030 m s^{-1}, respectively. Due to the limited sampling times and the uncertainties in the photochemical reaction rates of both O_3 and CO, the relative errors in these budget-based estimates are greater than 90%.

For the short-lived anthropogenically-influenced layer (below interface *B*) shown in Fig. 13, there is also little agreement between methods. However, the divergence method predicts a large negative entrainment initially at -0.040 m s^{-1} that increased in magnitude to -0.009 m s^{-1} before the layer became indistinguishable from layer *A*. The water mixing ratio flux method generally predicted values near zero.

The subsidence inversion (interface *C*) decreases in height with time, and the divergence method-based entrainment rates are less than -0.01 m s^{-1} for the entire Lagrangian as shown in Fig. 14. At JDT 204.9 (2130, 23 July), the divergence method predicted -0.021 m s^{-1}, but the mixing ratio flux method predicted 0.015 m s^{-1}, corresponding to a difference in magnitude of 0.036 m s^{-1}. The negative net entrainment predicted by the divergence method here is inconsistent with the existence of a turbulence-free layer above the subsidence inversion. This contradiction indicates that the divergence method is not appropriate here, suggesting that the difference in horizontal wind velocity at the inversion resulted in significant differential horizontal advection (which is assumed to be negligible in this approach).

6. Uncertainty analysis

The divergence and flux methods showed similar trends for entrainment, but the magnitudes often did not agree. The calculated entrainment rates are near the low end of the range of reported entrainment estimates (Stull, 1988; Russell et al., 1998). Both methods suffer from significant uncertainties which we describe here.

Lenschow et al. (1999) have studied the errors associated with the divergence approach for a 1000-m boundary layer for sampling statistics of an aircraft carrying similar turbulence instrumentation. Their calculations indicate that a single sampling time of 30 min would be expected to provide an uncertainty in entrainment of 0.1 m s^{-1} for a typical stratocumulus-capped boundary layer using the horizontal velocity integral scale obtained by Lenschow and Stankov (1986). For each stack used to calculate a divergence in this work, there are three to five consecutive sampling times of 28 min each, corresponding to predicted uncertainties of from 0.019 to 0.051 m s^{-1}, or relative errors from 98% to 1400%. Typical values of the uncertainties are between factors of 2 and 4 for a single stack. The number of boxes for each stack, the height of the layer interface during each stack, and the corresponding estimated error for each calculated entrainment rate are given in Table 1.

Since flight patterns consisted of boxes broken into four discontinuous sides, the accuracy of the calculation is also limited by the fact that the sampling was not strictly carried out as a closed-loop. In most instances, the distance of closest approach did not exceed 25 m at each intersection, for a total closing distance for the entire square of 100 m. Calculations of Lenschow et al. (1999) suggest that the associated error in the divergence for this offset would be less than 4×10^{-6} s^{-1}, which would result in a negligible contribution.

The finite time required to complete a single box pattern also results in a measurement which represents both a spatial and temporal average, subject to the variability in the boundary layer in both time and space. If we assumed that the changes in entrainment rates over multiple stacks and multiple flights were smaller than the uncertainties reported here for individual measurements, we can improve our sampling statistics by averaging at the expense of diminished time resolution. With this important caveat, we obtain entrainment rates for the interfaces directly below the free troposphere of 0.007, 0.007, and 0.006 m s^{-1} with errors of 0.013, 0.011, and 0.014 m s^{-1} for Lagrangians 1, 2, and 3, respectively. Here we

Table 2. *Entrainment rates and associated error estimates during the ACE-2 Lagrangian experiments calculated by the flux method*

Flight: stack	JDT	Δq_A (g kg^{-1})	Flux $(w'q')_A$ (g kg^{-1} m s^{-1})	Interface height, z_A (m)	Entrainment rate, w_e^A (m s^{-1})	Δq_B (g kg^{-1})	Flux $(w'q')_B$ (g kg^{-1} m s^{-1})	Interface height, z_B (m)	Entrainment rate, w_e^B (m s^{-1})	Δq_C (g kg^{-1})	Flux $(w'q')_C$ (g kg^{-1} m s^{-1})	Interface height, z_C (m)	Entrainment rate, w_e^C (m s^{-1})
Lagrangian 1													
A551: 1	185.02	−1.5	-2.8×10^{-02}	364	1.9×10^{-02} $\pm 1.8 \times 10^{-02}$								
A552: 1	185.49	−2.2	1.6×10^{-02}	719	-7.2×10^{-03} $\pm 2.2 \times 10^{-02}$	−6.4	2.8×10^{-02}	1394	-4.4×10^{-03} $\pm 1.4 \times 10^{-02}$				
A553: 1	185.94	−1.2	3.8×10^{-01}	881	-3.3×10^{-01} $\pm 1.5 \times 10^{-01}$	−8.2	2.0×10^{-01}	1068	-2.4×10^{-02} $\pm 1.3 \times 10^{-02}$				
Lagrangian 2													
A558: 1	198.00					−0.3	-5.5×10^{-03}	595	2.0×10^{-03} $\pm 1.3 \times 10^{-01}$				
A559: 1	198.46	−1.0	-2.3×10^{-02}	336	2.4×10^{-02} $\pm 2.6 \times 10^{-02}$	−2.8	-2.9×10^{-02}	1026	1.1×10^{-02} $\pm 2.5 \times 10^{-02}$				
A560: 1	198.95					−3.4	-8.9×10^{-03}	1053	2.6×10^{-03} $\pm 1.9 \times 10^{-02}$				
A560: 2	199.09					−6.1	-2.2×10^{-02}	1051	3.5×10^{-03} $\pm 1.1 \times 10^{-02}$				
Lagrangian 3													
A566: 1	204.49	−4.0	-1.4×10^{-02}	475	3.5×10^{-03} $\pm 7.6 \times 10^{-03}$	−5.8	4.1×10^{-04}	1667	-7.1×10^{-05} $\pm 1.7 \times 10^{-02}$				
A567: 1	204.93	−4.7	1.5×10^{-02}	488	-3.3×10^{-03}	−6.1	4.2×10^{-03}	1150	-7.0×10^{-04} $\pm 1.2 \times 10^{-02}$	1.3	1.9×10^{-02}	2023	1.5×10^{-02} $\pm 9.7 \times 10^{-02}$
A567: 2	205.10	−4.8	4.9×10^{-06}	762	-1.0×10^{-06} $\pm 9.6 \times 10^{-03}$								
A568: 1	205.43	−2.6	6.8×10^{-02}	950	-2.7×10^{-03} $\pm 2.3 \times 10^{-02}$					−5.6	1.6×10^{-02}	1446	-2.9×10^{-03} $\pm 1.7 \times 10^{-02}$
A568: 2	205.57	−3.2	4.8×10^{-02}	950	-1.5×10^{-03} $\pm 1.8 \times 10^{-02}$								

have averaged all individual measurements from both methods, except in the case of Lagrangian 3 where we have omitted the divergence method values since we believe them to be biased by differential horizontal advection. For the lowest interface (labelled *A* in each case), estimates of -0.024, 0.015, and $-0.001\ \mathrm{m\ s^{-1}}$ are recommended for Lagrangians 1, 2, and 3, respectively. For interface *B* in Lagrangian 3, we believe that $0.000\ \mathrm{m\ s^{-1}}$, that is, effectively no net entrainment, is the best estimate from the two methods we have considered here. For the low entrainment rates of less than $0.020\ \mathrm{m\ s^{-1}}$, the associated errors are still unacceptably high.

Typically, the height of the boundary layer can vary up to 100 m within the 40 km side-length boxes sampled here (Russell et al., 1998). In addition to the uncertainty in the height of the boundary layer, the jump in tracer concentration may be small or difficult to quantify. Inhomogeneous air masses may have added to the error in some data. Lenschow et al. (1999) have estimated the typical sampling error for the covariance values calculated by the flux method for a 1000-m boundary layer. We have used this estimate and incorporated the additional error associated with the measurement of the jump in concentration at the interface to provide the estimated relative errors given in Table 2. A small absolute value for the mixing ratio jump value of $-0.28\ \mathrm{g\ kg^{-1}}$ resulted in a large error of $0.13\ \mathrm{m\ s^{-1}}$ in the entrainment rate for flight A558 of Lagrangian 2. Also, profiles through the boundary layer top were only conducted at intervals separated by several hours. Under these conditions, detailed measurements of the characteristics at the interface were limited, increasing the uncertainty for these values.

In addition, for the layers in which we assumed that both layers had equal slopes where only one covariance rate was available for that layer, we have estimated the error introduced by this assumption to be the standard deviation of the covariance slopes from all layers measured during the project for which two or more values were available. The resulting uncertainties are much larger than the range of 5% to 25% relative error that would have been expected had we had sufficient data to quantify these slopes in all layers. We believe these conservative estimates of the error are appropriate here in light of the limited amount of information available.

In summary, the uncertainty in determining the difference in mixing ratio concentration at the boundary layer interface and the limited number of values per layer were frequently an important source of error for the flux method which made the divergence method a useful alternative approach, but the latter contained errors of a factor of two or more for entrainment velocities $\leqslant 0.01\ \mathrm{m\ s^{-1}}$. Additional data on the change in concentration across the interface would increase the accuracy of the covariance method. Longer sampling times would also have improved the divergence method estimates. In future experiments, at least two, preferably larger, boxes in each layer would improve the accuracy of both approaches, and circle patterns would improve the sampling efficiency for a fixed amount of flight time. Ideally, more stacks and more profiles are needed to obtain better sampling statistics on entrainment rates, but unfortunately extending the sampling time will increase the uncertainties due to temporal variations.

7. Acknowledgements

This analysis was supported by NSF grant ATM-9732949 and NASA grant NAG5-8676. The manuscript was improved greatly by the helpful comments of Donald Lenschow for which the authors express their thanks. This research is a contribution to the International Global Atmospheric Chemistry (IGAC) Core Project of the International Geosphere-Biosphere Programme (IGBP) and is part of the IGAC Aerosol Characterization Experiments (ACE).

REFERENCES

Albrecht, B. A., Penc, R. S. and Schubert, W. H. 1985. An observational study of cloud-topped mixed layers. *J. Atmos. Sci.* **42**, 800–822.

Bates, T. S., Huebert, B. J., Gras, J. L., Griffiths, F. B. and Durkee, P. A. 1998. The International Global Atmospheric Chemistry (IGAC) Projects' First Aerosol Characterization Experiment (ACE 1): overview. *J. Geophys. Res.* **103**, 16,297–16,318.

Bretherton, C. S., Austin, P. and Siems, S. T. 1995. Cloudiness and marine boundary layer dynamics in

the ASTEX Lagrangian experiments: Part II: cloudiness, drizzle, surface fluxes, and entrainment. *J. Atmos. Sci.* **52**, 2724–2735.

Durkee, P. A., Nielsen, K. E., Russell, P. B., Schmid, B., Livingston, J. M., Collins, D., Flagan, R. C., Seinfeld, J. H., Noone, K. J., Öström, E., Gass, S., Hegg, D., Bates, T. S., Quinn, P. K. and Russell, L. M. 2000. Regional aerosol properties from satellite observations: ACE-1, TARFOX and ACE-2 results. *Tellus* **52B**, 484–497.

Johnson, D. W., Osborne, S., Wood, R., Suhre, K., Andreae, M. O., Johnson, R., Businger, S., Quinn, P. K., Bates, T. S., Durkee, P. A., Russell, L. M., Noone, K., Glantz, P., Bandy, B., O'Dowd, C., Rapsomanikis, S. and Rudolph, J. 2000a. An overview of the Lagrangian experiments undertaken during the North Atlantic Regional Aerosol Characterisation Experiment (ACE-2). *Tellus* **52B**, 290–320.

Johnson, D. W., Osborne, S., Wood, R., Suhre, K., Quinn, P. K., Bates, T. S., Öström, E., Andreae, M. O., Noone, K., Glantz, P., Bandy, B., Rapsomanikis, S., Rudolph, J. and O'Dowd, C. 2000b. Observations of the evolution of the aerosol, cloud and boundary layer characteristics during the first ACE-2 Lagrangian experiment. *Tellus* **52B**, 348–374.

Kawa, S. R. and Pearson, Jr., R. 1989. An observational study of stratocumulus entrainment and thermodynamics. *J. Atmos. Sci.* **46**, 2649–2661.

Lenschow, D. H. 1996. A proposal for measuring entrainment into the cloud-capped boundary layer. In: *Proceedings of the ETL/CSU Cloud-related process modeling and measurement workshop, Boulder, Colorado, 23–25 October 1995* (eds. Frisch, A. S., Randall, D. A. and Schubert, W. H.). NOAA ETL Report, pp. 29–55, Natl. Oceanic and Atmos. Admin., Silver Spring, Md.

Lenschow, D. H. and Stankov, B. B. 1986. Length scales in the convective atmospheric boundary layer. *J. Atmos. Sci.* **43**, 1198–1209.

Lenschow, D. H., Krummel, P. B. and Siems, S. T. 1999. Measuring entrainment, divergence, and vorticity on the mesoscale from aircraft. *J. Atmos. Oceanic Tech.*, in press.

Lilly, D. K. 1968. Models of cloud-topped mixed layers under a strong inversion. *Quart. J. Roy. Meteor. Soc.* **94**, 292–309.

Martin, G. M., Johnson, D. W. and Spice, A. 1994. The measurement and parameterization of effective radius of droplets in warm stratocumulus clouds. *J. Atmos. Sci.* **51**, 1823–1842.

Nicholls, S. 1984. The dynamics of stratocumulus: Aircraft observations and comparisons with a mixed layer model. *Quart. J. Roy. Meteor. Soc.* **113**, 783–820.

Osborne, S. R., Johnson, D. W., Wood, R., Bandy, B. J., Andreae, M. O., O'Dowd, C. D., Glantz, P. and Noone, K. J. 2000. Observations of the evolution of the aerosol, cloud and boundary layer dynamic and thermodynamic characteristics during the second Lagrangian experiment of ACE-2. *Tellus* **52B**, 375–400.

Raes, F. 1995. Entrainment of free tropospheric aerosols as a regulating mechanism for cloud condensation nuclei in the remote marine boundary layer. *J. Geophys. Res.* **100**, 2893–2903.

Raes, F., Bates, T. S., McGovern, F. M. and Van Liedekerke, M. 2000. The second Aerosol Characterization Experiment (ACE-2): general overview and main results. *Tellus* **52B**, 111–126.

Raes, F., Van Dingenen, R., Wilson, J. and Saltelli, A. 1993. Cloud condensation nuclei from dimethyl sulphide in the natural marine boundary layer: remote versus in-situ production. In: *Dimethylsulphide: oceans, atmosphere and climate*, pp. 311–322.

Russell, L. M., Lenschow, D. H., Laursen, K. K., Krummel, P. B., Siems, S. T., Thornton, D. C., Bandy, A. R. and Bates, T. S. 1998. Bidirectional mixing in an ACE1 marine boundary layer. *J. Geophys. Res.* **103**, 16,411–16,432.

Russell, L. M., Pandis, S. N. and Seinfeld, J. H. 1994. Aerosol production and growth in the marine boundary layer. *J. Geophys. Res.* **99**, 20,989–21,003.

Stull, R. B. 1988. *An introduction to boundary layer meteorology*. Kluwer Academic Press, Dordrecht, 670 pp.

Van Dingenen, R., Raes F., Putaud, J.P., Virkkula, A. and Mangoni M. 1999. Processes determinig the relationship between aerosol number and non-sea-salt sulfate mass concentrations in the clean and perturbed marine boundary layer. *J. Geophys. Res.* **104** (D7), 8027–8038.

Van Dingene, R., Virkkula, A.O. and Raes F. 2000. A simple non-linear analytical relationship between aerosol accumilation number and sub-micron volume, explaining their observed ratio in the clean and polluted marine boundary layer. *Tellus* **52B**, 439–451.

Verver, G., Raes, F., Vogelezang, D. and Johnson, D. 2000. The second Aerosol Characterization Experiment (ACE-2): meterological and chemical context. *Tellus* **52B**, 126–140.

Wang, Q., Lenschow, D. H., Pan, L., Schillawski, R. D., Kok, G. L., Prevot, A. S. H., Laursen, K. K., Russell, L. M., Bandy, A., Thornton, D. and Suhre, K. 1999. Characteristics of the marine boundary layer observed during Lagrangian measurements, Part 2: Turbulence structure. *J. Geophys. Res.* **104**, 21,767–21,784.

Wood, R., Johnson, D. W., Osborne, S. R., Bandy, B. J., Andreae, M. O., O'Dowd, C. D., Glantz, P. and Noone, K. J. 2000. Boundary layer, aerosol and chemical evolution during the third Lagrangian experiment of ACE-2. *Tellus* **52B**, 401–422.